Development and performance evaluation of an electromagnetic tracking system for surgery navigation

Published Source
G. Andria, F. Attivissimo, A. Di Nisio, A.M.L. Lanzolla, P Larizza and S. Selicato, "Development and performance evaluation of an Electromagnetic Tracking System for surgery navigation", Measurement, vol. 148, pp.1-7, December 2019, https://doi.org/10.1016/j.measurement.2019.106916.

Development and performance evaluation of an Electromagnetic Tracking System for surgery navigation

Gregorio Andria[1], Filippo Attivissimo[1], Attilio Di Nisio[1], Anna Maria Lucia Lanzolla[1], Pietro Larizza[2], Sergio Selicato[1]

Department of Electrical and Information Engineering Polytechnic University of Bari
[gregorio.andria, filippo.attivissimo, attilio.dinisio, anna.lanzolla,]@poliba.it, selicato.sergio@gmail.com

Masmec Biomed Spa, Bari, Italy
pietro.larizza@masmec.com

***Abstract*—In Image Guided Surgery, an electromagnetic tracking system is used nowadays to locate surgical instruments in the patient's anatomical 3D model. In this work we illustrate the development and the evaluation of a new Electromagnetic Tracking system (EMTS) able to provide a large tracking volume.**

The innovation of this proposed EMTS consists in the development of the Field Generator (FG), which includes five properly designed coils. Attention has been paid to the magnetic field generated by each coil in order to comply with the safety limits imposed by IEEE Stds C95.1 and C95.6. The simultaneous transmission of the five coils is possible thanks to a suitable frequency division multiplexing.

To validate the proposed design, a detailed noise analysis was performed with several experimental tests in different working conditions with the aim of evaluating measurement errors.

Actual performance of the system in reconstructing sensor position has been quantified by using a suitable interpolation technique. In particular, mean position error and standard deviation were evaluated for different distances of magnetic sensor from field generator.

***Index Terms*—Surgery navigation, electromagnetic tracking, field generator, tracking volume, sensor coil.**

I. INTRODUCTION

Computer-assisted medical interventions are increasingly used in modern surgery because they offer many benefits compared to conventional approaches, including increased accuracy, reduction

of postoperative pain, reduction of complications and risks for the patient, and decreased hospitality time.

This technique is based on the navigation of the surgery tool in a three-dimensional anatomical model [1]-[3] of the patient built with a data fusion of diagnostic images such as computerized tomography (CT), magnetic resonance imaging (MRI), Positron Emission Tomography (PET) and Ultrasound (US) [4]-[9]. Then, the surgeon inserts the tools in human body of patient and observes its movement in anatomical model on display.

In order to capture the movements of the tools, a tracking system that measures their position and orientation in a known reference system is used. Tracking systems are classified taking into account the physical principle on which they are based [10]. In surgery navigation, most used tracking systems are optical and electromagnetic.

Optical tracking systems (OTS) include one or more cameras and a set of dedicated markers applied to the object. These systems offer high accuracy, a very important feature in surgical procedures. However, since cameras and markers should be in line-of-sight, any obstacle between them makes tracking difficult or impossible, hence these systems can't be used for intra-corporal interventions.

Electromagnetic tracking systems (EMTS) determine the position and the orientation of the target object by means of measurement of magnetic field with known geometry. For this purpose, a small sensor coil, measuring the amplitude of magnetic fields generated by a field generator (FG), is inserted into a surgery tool. The very small dimensions of the magnetic sensor (MS) and the independence from line-of-sight, overcome the limitations of OTS, so allowing the use of EMTS in many intervention areas such as neurosurgery [11],[12] oncology [13], laparoscopy [14] and maxillofacial surgery [15]. The accuracy and resolution of these tracking devices are slightly lower than OTS but quite acceptable for surgery navigation applications. However, the presence of ferromagnetic materials and electronic devices near the field generator causes a distortion of the reference magnetic field and it provides dynamic and static errors in both position and orientation measurement [16], [17]. Therefore, different methods have been developed [18]-[20] to make EMTS less affected by EM interferences.

The aim of this work is the realization of a suitable EMTS device with high resolution with operating distance of 1 m, high reliability and high measurement sensitivity. To obtain these characteristics a new field generator including an increased number of transmitting coils that are suitable arranged was developed.

This paper is structured as follows: Section II explains working principle and the architecture of the developed system. Section III is centered on noise characterization of tracking system including the evaluation of noise level and of statistical distribution of measurement errors. In Section IV the interpolation method used to evaluate sensor position was explained and the experimental results obtained in different working conditions were reported. Finally, Section V summarizes the performance of the developed tracking system and indicates future actions to improve system accuracy

II. Experimental set-up of EMTS

Italian company MASMEC Biomed, in collaboration with Polytechnic University of Bari, has developed a new electromagnetic tracking system to be integrated in IGS systems. Its peculiarity is a tracking volume larger than actual EMTSs in commerce such as Aurora® system by NDI [21] which is the most used system in surgical navigation and allows a maximum distance of surgical tools from FG of 500 mm. For this aim, experimental tests for system validation were performed at distances 0.6 m and 1 m from FG.

The architecture, shown in Fig.1, was described in [22],[23]. It includes three essential components:

- Field Generator (FG): it includes five coils that generate AC magnetic fields;
- Magnetic Sensor (MS): Aurora 6DOF Probe [24], a coil of small size, similar to a needle (shown in Fig. 2);
- Control Unit: it is dedicated to the generation of power signals for the FG and to the acquisition and processing of measurement data from the sensor coil.

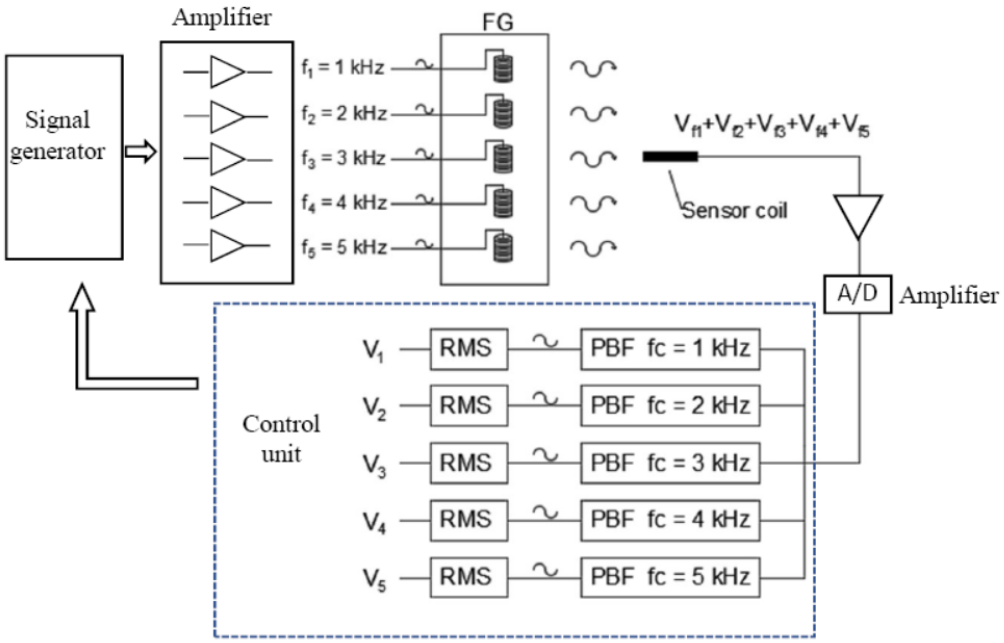

Fig. 1 Architecture of the EMTS.

77

78

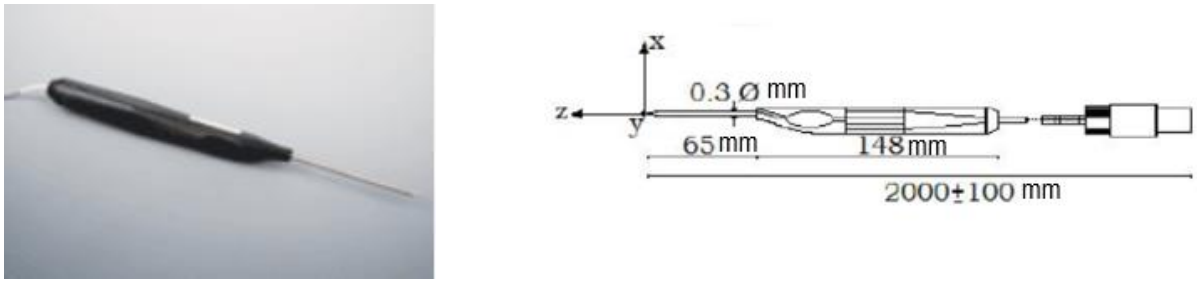

Fig. 2 Scheme and picture of used magnetic sensor

79 The proposed system is based on Frequency Division Multiplexing (FDM) [13]. Five used coils
80 are powered by sinusoidal signals with five different frequencies of approximately 1, 2, 3, 4 and 5
81 kHz, respectively.

82 Each magnetic field induces on the MS a sinusoidal voltage with different frequencies and an
83 amplitude depending on both the position and the orientation of the MS. To obtain each signal
84 component, the MS output is filtered by means of a suitable pass-band filter, as shown in Fig. 1.

For this aim a new field generator was designated to provide appreciable magnetic fields at a suitable distance from it. The five FG coils are fixed on a dedicated non-metal platform to avoid the generation of secondary magnetic fields that may produce EM interferences.

The coils have been arranged so that the first three are along the Cartesian axes and the others two are inclined by 45° with respect to the support plane, as shown in Fig.3. In this way, it is possible to enlarge the tracking volume, ensuring at same time that the contribution of mutual inductances is negligible.

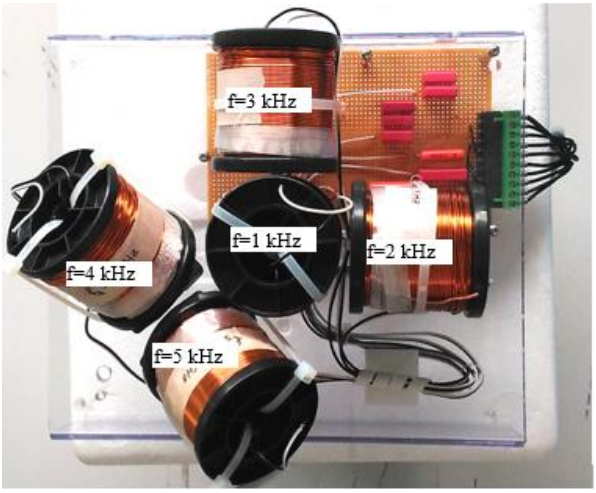

Fig. 3 Arrangement of the five coils.

The design of each single coil takes into account the IEEE Std. C95.6 [25] and Std. C95.1 [26] that define the security limits for the exposure to magnetic fields, in controlled environments, of limbs, torso and head. The legislation imposes the maximum amplitude of a sinusoidal magnetic field the human body can be subjected to. These limits change according to the frequency range of the magnetic fields, as shown in TABLE 1.

TABLE I. IEEE STANDARDS FOR EM FIELD EMISSION IN THE RANGE 0 - 300 GHZ.

Std. C95.6-2002: 0 -3 kHz	*Hrms* (A/m)	*Brms* (mT)
Threshold for limbs	4000	5.03
Threshold for torso and head	2000	2.51

Std. C95.1-2005: 3 kHz – 5 MHz	*Hrms* (A/m)	*Brms* (mT)
Threshold for limbs	900	1.13
Threshold for torso and head	163	0.205

In this proposed system, the threshold value of 0.2 mT is considered because it refers to the more restrictive case. To respect this condition different simulation tests, detailed in a previous study [27], have been performed to evaluate the best physical parameters of transmitting coils and the best current value. In particular, the following parameters were selected as shown in Fig. 4: length coil l=45 mm, internal radius r_1= 12 mm. external radius r_2= 19 mm, number of turns N_t=315, current value I=1.5 A. With these parameters the security limits are respected just outside the FG, at a distance of 150 mm from its center.

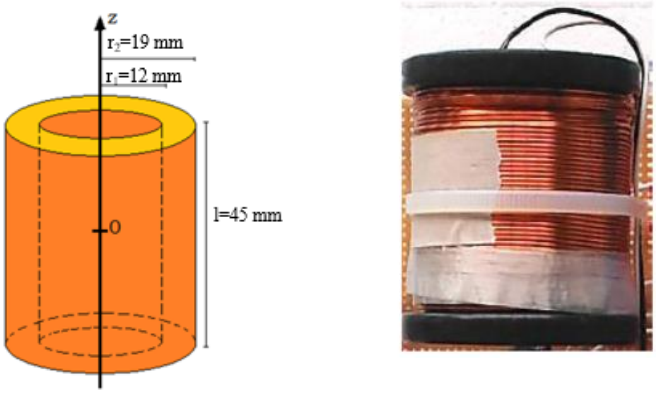

Fig. 4 Scheme and picture of used magnetic sensor

The AC power signals for the coils of the FG are generated by a DAQ module, model NI 9263 by National Instruments. Since the supplied power is limited, it is necessary to use a power amplifier stage for each coil, obtained with a Texas Instrument OPA 544 operational amplifier in non-inverting configuration with a gain equal to 51. Sensor signal was amplified by means of instrumentation amplifier INA 114 by Texas Instruments

Preliminary experimental results have shown that the overheating of coil resistances provides magnetic field variations that significantly affect the measurement data. Therefore, a suitable control loop on coil currents was implemented to maintain the magnetic field constant [22]. Current measurements were performed by means of magnetic sensors. Experimental tests have proved a good stability of current signal, showing a standard deviation of about 0.01% (for almost all FG coils). Moreover, it should be considered that there is an FG transient, after power- on, which lasts about twenty seconds.

To manage and control the proposed system, it is necessary a control unit that generates the five sinusoidal signals for the field generator and acquires the voltage outputs from the current sensors and from the MS. An experimental set-up based on a DAQ (Data Acquisition) module and software interface was developed.

The management software was developed in LabVIEW® (by National Instruments Corp.) which permits to easily integrate different acquisition devices.

The developed software includes two fundamental tasks:

i. Generation of the power signals for the FG with feedback in order to keep constant the reference magnetic field.

ii. Acquisition and elaboration of voltages induced on MS and current sensors.

Five digital IIR (Infinite Impulse Response) filters were used for noise reduction and separation of components in MS signals. In particular, Butterworth passband filters with order 30, bandwidth 50 Hz, pass band ripple 1 dB and attenuation 60 dB were applied. Each filter was centered on a different excitation frequency of the FG, from about 1 kHz to 5 kHz.

III. Noise Analysis

After prototyping, a noise characterization of the tracking system was performed. The electromagnetic tracking system, within the IGS system, acts as a measuring device to provide the position and orientation of the surgical tool.

The context where the IGS works is very delicate because there are many critical anatomical entities, such as arteries or nervous fibers, and any error in surgical tool position can lead to serious and sometimes irremediable damages. Hence, for IGS systems, it becomes very important to provide accurate measurement data.

The voltage signal at the output of the MS is decomposed into its components, according to the scheme of Fig. 1, so obtaining the five rms values, $v_1(t)$,…,$v_5(t)$, that are analyzed as follows.

A detailed study of statistical proprieties of induced voltage signals was carried out to characterize the accuracy and repeatability of the tracking system in different working conditions. Three distances of the MS from the FG were considered: 0.2, 0.6 and 1 m. For the experimental tests, an anthropomorphic robot manufactured by KUKA assuring a positioning repeatability of 0.03 mm, shown in Fig. 6, was used to provide a specific trajectory for system testing.

The EMTS sensor is placed at the end of a carbon pole mounted on Kuka’s arm in order to minimize the EM interferences. In the assignment of the Cartesian coordinates of trajectories

performed by the Kuka robot, an offset value which takes into account of the carbon pole length (1 m) was considered.

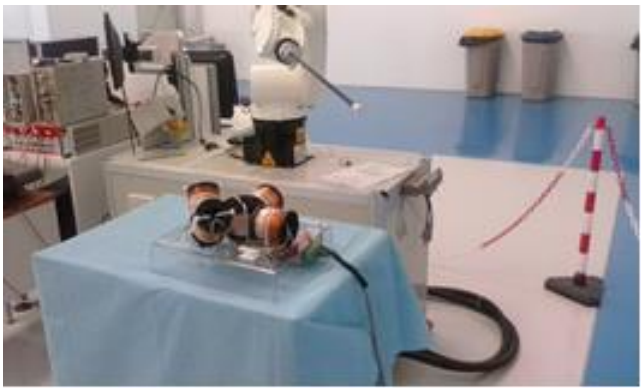

Fig. 5 Experimentation with the KUKA robot.

The trajectory performed by the Kuka robot consisting of 27 points within cubic volumes whose centers were at the three distances given above. For each point of the analyzed trajectory, two hundred repeated measures of each signal v_i, i=1,…,5, were acquired with a sampling period equal to 50 ms.

A statistical study was performed on this set of measurements and the dispersion was evaluated by calculating the standard deviation.

In particular, by analyzing the acquisition data when FG is turned off, it is possible to evaluate noise contribution by analyzing standard deviations (std) of sampled $v_i(t)$.

TABLE II. lists the standard deviations averaged for the points relevant to the same cube. In this case the std relevant to each signal is about 5 μV and is not dependent upon distance.

TABLE II. STD WITH FG OFF, AS A FUNCTION OF CUBE DISTANCE AND FREQUENCY

std (mV rms)	1 kHz	2 kHz	3 kHz	4 kHz	5 kHz
0.2 m	0.0048	0.0052	0.0051	0.0048	0.0047
0.6 m	0.0048	0.0050	0.0050	0.0049	0.0047
1 m	0.0054	0.0056	0.0055	0.0049	0.0047

Moreover, by observing error distributions, it is possible to note that, to the first approximation, the measurement process is Gaussian, as shown in Fig. 8.

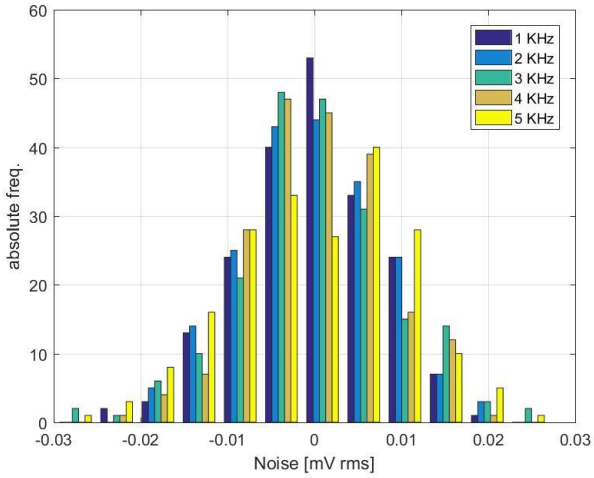

Fig. 6 Error distribution at 0.6 m from FG, with FG turned off. Data relevant to different frequencies are indicated with different colors.

Successively, experimental tests with the FG turned on were performed to evaluate the noise influence on measurement signal.

TABLE III. SENSOR SIGNAL COMPONENTS AND RELATIVE ERROR AT 0.6 M

Frequency (kHz)	1	2	3	4	5
Sensor signal (mV rms)	0.32	13	4.8	6.9	12
Relative error %	1.50%	0.04%	0.10%	0.07%	0.04%

The root mean square values of MS components, $v_i(t)$, were measured for different distances and compared with std values listed in TABLE II. Experimental results highlight that noise effect due to devices used for acquisition signal is always negligible. As an example, TABLE III. shows the results obtained for the 0.6 m distance where the relative errors were evaluated by means of the ratio between the sensor signal components when the FG is on and standard deviation values obtained with FG turned off.

IV. POSITION ESTIMATION

As already described, the developed system measures the magnetic field generated by the FG, which is the superposition of different components at frequencies $f_1, \dots, f_5$, by using a MS. Voltage output from MS is filtered numerically in order to give rms values at that frequencies, denoted as $\boldsymbol{v} = [v_1, \dots, v_5]$. In this section, the problem is faced of finding the position of the MS, $\boldsymbol{r} = [x, y, z]$, as a function of sensor data $\boldsymbol{v}$. *x*-, *y*- and *z*-axis are oriented in the same directions of the three orthogonal coils of the FG (see Fig. 3), with the z-axis aligned vertically. The function relating $\boldsymbol{v}$ to

$\boldsymbol{r}$ will not be given in a simple closed form, it will represent abstractly, instead, the application of a numeric algorithm. We will use arrays $\boldsymbol{R}$ and $\boldsymbol{V}$ to denote, respectively, sets of positions and sensor readings, concatenated vertically.

A. Interpolation method

Position estimation is based on interpolation between calibration points. During calibration, the MS is placed in M^c different known positions $\boldsymbol{r_i^c} = [x_i^c, y_i^c, z_i^c], i = 1, \dots, M^c$ which can be collected into an $M^c \times 3$ array

$$\boldsymbol{R}^c = \begin{bmatrix} x_1^c & y_1^c & z_1^c \\ \dots & \dots & \dots \\ x_{M^c}^c & y_{M^c}^c & z_{M^c}^c \end{bmatrix} \tag{1}$$

For each position, corresponding sensor readings are obtained $\boldsymbol{v_i^c} = [v_{i1}^c, \dots, v_{i5}^c], i = 1, \dots, M^c$, which are quintuples of rms voltage. They can be referred as $M^c \times 5$ array

$$\boldsymbol{V}^c = \begin{bmatrix} v_{11}^c & \dots & v_{15}^c \\ \dots & \dots & \dots \\ v_{M^c 1}^c & \dots & v_{M^c 5}^c \end{bmatrix} \tag{2}$$

Afterward, for any new measured sensor reading $\boldsymbol{v'}$, the interpolated position $\boldsymbol{r'} = [x', y', z']$ is found by processing $(\boldsymbol{V^c}, \boldsymbol{R^c}, \boldsymbol{v'})$ data:

$$\boldsymbol{r'} = \boldsymbol{g}(\boldsymbol{V^c}, \boldsymbol{R^c}, \boldsymbol{v'}) \tag{3}$$

In particular, calibration points shown in Fig. 7 are interpolated by using triangulation and piecewise linear interpolation. In a first step, Delaunay triangulation is applied to $\boldsymbol{V^c}$, so obtaining a set of simplices. Successively, the simplex that contains $\boldsymbol{v'}$ is selected, let $(s_1, \dots, s_6)$ be the indices of its vertices $(\boldsymbol{v}_{s_1}, \dots, \boldsymbol{v}_{s_6})$. Finally, linear interpolation is calculated by weighting values $(\boldsymbol{r}_{s_1}, \dots, \boldsymbol{r}_{s_6})$ according to the barycentric coordinates of $\boldsymbol{v'}$ inside the simplex $(\boldsymbol{v}_{s_1}, \dots, \boldsymbol{v}_{s_6})$ [28],[29].

Clearly, position estimation can be performed only for sensor readings that are inside the triangulation of $\boldsymbol{V}^c$.

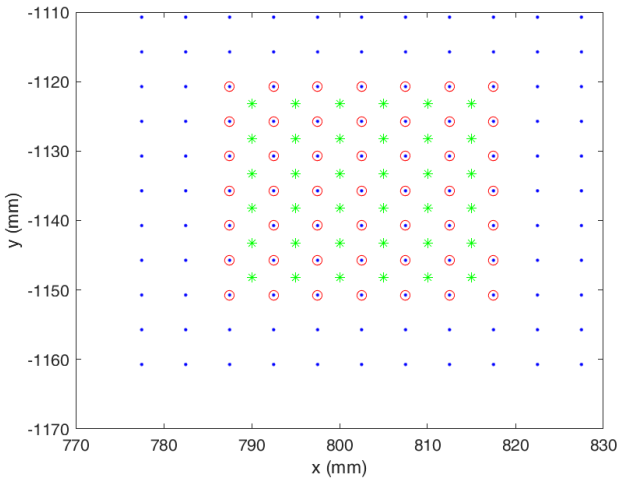

Fig. 7 - Projection on the XY plane of MS points at 0.6 m from the FG: (blue dots) calibration points; (red circles) points for test a; (green stars) points for test b.

B. Experimental results

The proposed tracking system was calibrated and its performance was evaluated at several distances from the FG, up to about 1 meter.

In a first series of experiments, calibration was performed on a regular grid inside a cubic volume at a mean distance of 0.6 m from the FG, with a grid step of 5 mm along each direction and an edge length of 50 mm, for a total of M^c =1331 points. Spatial coordinates of calibration points are illustrated in Fig. 7 with red circles. The MS was moved by means of the already mentioned KUKA robot. For each calibration point, MS positions where recorded into $\boldsymbol{R}^c$, and $N = 200$ sensor readings where averaged, so obtaining $\boldsymbol{V}^c$.

After calibration, two tests, indicated as test *a* and test *b*, were performed to determine position estimation error.

In test *a*, the MS was placed in test points which were a subset of size M^a of the previously used calibration positions. In particular, a subcube with 7 points along each edge, spaced by 5 mm, was selected, leaving a margin of two points (10 mm) with respect to each face of the calibration cube, as shown in Fig. 7. Let $\boldsymbol{r}_i^a = [x_i^a, y_i^a, z_i^a]$ and $\boldsymbol{v}_i^a = [v_1^a, \dots, v_5^a], i = 1, \dots, M^a$ be the MS sensor positions and readings, respectively. By using the previously defined interpolation method, positions $\boldsymbol{r}_i' = [x_i', y_i', z_i']$ were also estimated by means of

$$\boldsymbol{r}_i' = \boldsymbol{g}(\boldsymbol{V}^c, \boldsymbol{R}^c, \boldsymbol{v}_i^a) \tag{4}$$

Positions were estimated correctly, as shown in Fig. 8.

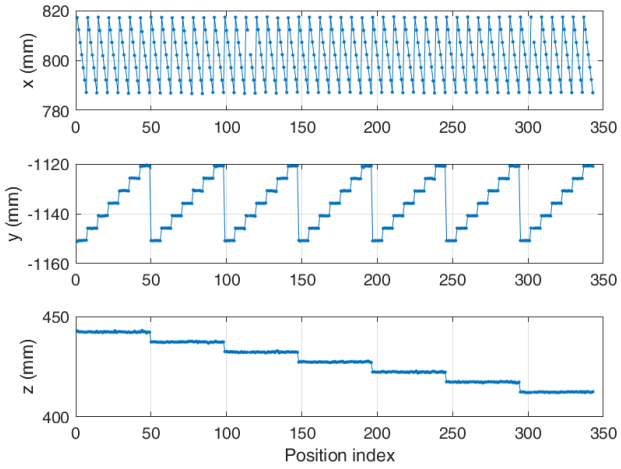

Fig. 8 Estimated positions at about 0.6 m from FG, as a function of index i.

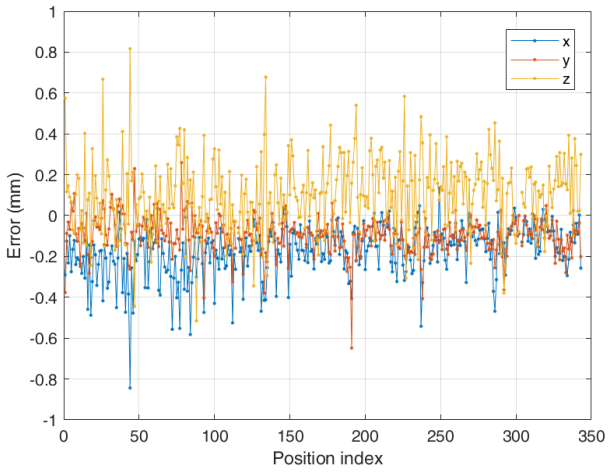

Fig. 9 Position estimation errors for each axis, as functions of point index i.

Estimation errors were calculated as $\boldsymbol{e_i} = [e_{xi}, e_{yi}, e_{zi}] = [x_i' - x_i^a, y_i' - y_i^a, z_i' - z_i^a]$. They are shown in Fig. 11. The Euclidean distance between $\boldsymbol{r}_i'$ and $\boldsymbol{r}_i$,

$$\|\boldsymbol{e}_i\| = \sqrt{{e_{xi}}^2 + {e_{yi}}^2 + {e_{zi}}^2} \tag{5}$$

was also used to evaluate system performance. Data shown in that figures are summarized by calculating the statistics of e_{xi}, e_{yi}, e_{zi} and $\|\boldsymbol{e}_i\|$, which are reported in the left side of TABLE IV.

It was assumed that error distributions did not change significantly among test points due to the small considered volume, hence statistics were calculated by varying the test point in that volume.

TABLE IV. POSITION ESTIMATION ERROR AT 0.6 M FROM FG

	Test a				Test b			
	e_x	e_y	e_z	$\|\|e\|\|$	e_x	e_y	e_z	$\|\|e\|\|$
mean (mm)	-0.17	-0.10	0.10	0.29	-0.42	-0.24	0.44	0.67
std (mm)	0.13	0.09	0.18	0.16	0.14	0.09	0.16	0.18
max (mm)	0.84	0.65	0.82	1.20	1.14	0.54	0.95	1.47
90*th* percentile	---	---	---	0.50	---	---	---	0.92

TABLE V. POSITION ESTIMATION ERROR AT 1 M FROM FG

	Test a				Test b			
	e_x	e_y	e_z	$\|\|e\|\|$	e_x	e_y	e_z	$\|\|e\|\|$
mean (mm)	-0.16	0.28	-2.52	2.73	-0.20	0.32	-3.55	3.67
std (mm)	0.26	0.54	1.82	1.64	0.28	0.53	1.72	1.63
max (mm)	1.07	2.02	9.17	9.39	1.01	1.89	8.72	8.76
90*th* percentile	---	---	---	5.05	---	---	---	5.81

The mean and the std of the Euclidean distance were 0.29 mm and 0.16 mm, respectively. Error along the different axis where of the same magnitude. These results are encouraging by taking into account that Aurora accuracy performance relevant to error position are 0.48 mm and 0.88 mm for standard uncertainty and uncertainty with 95% confidence interval, respectively [21].

It is noteworthy that position estimation by means of interpolation was not possible for 0.6 % of tested positions. In that cases, no containing simplices were found, i.e. relevant sensor readings $\boldsymbol{v}_i^a$ were outside the triangulation of $\boldsymbol{V}^c$. The probability of incurring in such circumstances is lowered if test points are well inside the calibration cube $\boldsymbol{R}^c$. Indeed, a distance of 1 cm from calibration boundaries was maintained, as already mentioned. During real magnetic tracking system usage, the proximity to calibration boundaries may be signaled and, when interpolation is not possible because $\boldsymbol{v}_i^a$ lies outside $\boldsymbol{V}^c$**,** the nearest calibration sensor readings among $\boldsymbol{V}^c$ may be found and its corresponding calibration position returned.

In the second test, referenced as *b*, the MS was placed in positions $\boldsymbol{r}_i^b$ different from the calibration ones, obtaining sensor readings $\boldsymbol{v}_i^b$ **,** $i = 1, \dots, M^b$. Positions were chosen on a regular

grid displaced by half-step with respect to the calibration grid, obtaining a cube which is at the center of the calibration volume, see green stars in in Fig. 7. Such positions were chosen in order to maximize distance from calibration points, with the aim of evaluating errors in nearly worst-case conditions. Error statistics are reported in the right side of TABLE IV. By comparison to the results obtained in test *a*, Euclidean error increased, reaching a mean of 0.67 mm and a std of 0.18 mm. It should be noted that, while test *a* puts in evidence repeatability errors due to noise and drift, test *b* includes also error contributions due to the performance of piecewise linear interpolation.

In a second series of experiments, calibration was performed at a mean distance of 1 m from the FG, inside a cube having the same size and number of points of the experiment at 0.6 m. Estimation error was calculated, as before, for two sets of test points. The first one (test *a*) was a subset of the calibration points, while the second one (test *b*) contains only points that are half-step between calibration ones. Results are reported in TABLE IV. Mean and std of Euclidean errors increased by comparison to errors at 0.6 m, reaching a mean of 2.7 mm and 3.7 mm for test *a* and test *b*, respectively. This is a consequence of decaying magnetic fields at increased distance. Moreover, it should be noted that the error is greater along z-axis than along *x*- and *y*-axes.

I. Conclusion

In this work, an innovative EMTS has been developed with the aim to provide a tracking volume greater than existing EM tracking devices integrated in IGS systems. A new field generator has been developed with an innovative architecture in order to produce appreciable reference magnetic fields beyond a distance of 0.6 m from it. Each FG coil has been designed in full compliance with IEEE safety standards for human body exposure to magnetic fields.

Coil excitation current was kept constant by means of a control loop[22]. A suitable software interface, developed in LabVIEW® ambient, provides controlled generation of the power signals of the FG, and digital parallel pass-band filtering (IIR) of the MS signal.

A position estimation technique was experimented, based on triangulation and piecewise interpolation of MS rms voltage readings. Despite its simplicity, it was able to provide accurate position measurements at 0.6 m from the FG, with a mean error of 0.29 mm and a std of 0.16 mm. However, performance decreased at 1 m from the FG, giving errors of a few millimeters; this was due mainly to increased errors along z-axis, which will be the subject of a further study.

Aknowledgement

This work, was supported by project SINACH, “Integrated minimally-invasive surgical navigation systems”, funded by European Regional Development Fund, POR Puglia FESR - FSE 2014-2020, “InnoNetwork” call.

REFERENCES

[1] Eric Grimson, Micheal Leventon, Liana Lorigo, Tina Kapur, Ron Kikinis, “Image Guided Surgery”, Scientific American, 1999, 280(6):62-9.

[2] Z, Ren, W.Q. Yang, “Development of a Navigation Tool for Revision Total Hip Surgery Based on Electrical Impedance Tomography”, IEEE Transactions on Instrumentation and Measurement ,vol. 65, no. 12, December 2016, pp. 2748-2757

[3] P. Zhou, Y. Liu, Y Wang,“Pipeline architecture and parallel computation-based real-time stereovision tracking system for surgical navigation”, IEEE Transactions on Instrumentation and Measurement, vol. 59, no 5, May 2010, pp. 1240-1250

[4] Xiaozhao Chen, Nan Bao, Jianhua Li, Yan Kang, “A Review of Surgery Navigation System Based on Ultrasound Guidance”, Proceeding of the IEEE International Conference on Information and Automation Shenyang, China, June 2012.

[5] G. Andria, F. Attivissimo, A Di Nisio, A.M.L Lanzolla., A Maiorana, M Mangiantini, M. Spadavecchia “Dosimetric Characterization and Image Quality Assessment in Breast Tomosynthesis,” IEEE Transactions on Instrumentation and Measurement, vol. 66, no. 10, pp. 2535-2544, Apr. 2017.

[6] G. Bachar, J.H. Siewerdsen, M.J. Daly, D.A. Jaffray, J.C. Irish, “Image quality and localization accuracy in C-arm tomosynthesis-guided head and neck surgery,” Med. Phys., vol. 34, no. 12, pp. 4664–4677, Nov. 2007.

[7] N. Casap, E. Tarazi, A. Wexler, U. Sonnenfeld, J. Lustmann, “Intraoperative computerized navigation for flapless implant surgery and immediate loading in the edentulous mandible,” International Journal of Oral & Maxillofacial Implants, vol. 20, no. 1, pp. 92-98, 2005.

[8] G. Andria, F. Attivissimo, G. Cavone, A.M.L. Lanzolla "Acquisition Times in Magnetic Resonance Imaging: Optimization in Clinical Use” IEEE Transactions on Instrumentation and Measurement, vol. 58, no. 9, pp. 3140-3148,. September 2009.

[9] G. Andria, F. Attivissimo, A. Di Nisio, A.M.L. Lanzolla, G. Guglielmi, R. Terlizzi, "Dose optimization in chest radiography: System and model characterization via experimental investigation", IEEE Transactions on Instrumentation and Measurement, vol. 63, no. 5, pp. 1163-1170, Oct. 2014.

[10] Greg Welch, Eric Foxlin, “Motion tracking: No silver Bullet, but a Respectable Arsenal”, IEEE Computer Graphics and Applications, vol.: 22, no: 6, Nov.-Dec. 2002.

[11] A. Vaccarella, E. De Momi, A. Enquobahrie,G. Ferrigno, “Unscented Kalman filter based sensor fusion for robust optical and electromagnetic tracking in surgical navigation”, IEEE Transactions on Instrumentation and Measurement, vol. 62, no. 7, 2013, pp. 2067-2081

[12] O. Suess, Th. Kombos, R. Kurth1, S. Suess, S. Mularski, S. Hammersen, M. Brock, “Intracranial Image-Guided Neurosurgery: Experience with a new Electromagnetic Navigation System”, Acta Neurochirurgica, , vol. 143, no 9, 2001

[13] Fang-Yi Liu, Xiao-Ling Yu, Ping Liang, Zhi-Gang Cheng, Zhi-Yu Han, Bao-Wei Dong, Xiao-Hong Zhang, “Microwave ablation assisted by a real-time virtual navigation system for hepatocellular carcinoma undetectable by conventional ultrasonography”, European Journal of Radiology, 2012, 81(7).

[14] Thomas Langø, Sinara Vijayan, Anna Rethy, Cecilie Våpenstad, Ole Vegard Solberg, Ronald Mårvik, Gjermund Johnsen, Toril N. Hernes, “Navigated laparoscopic ultrasound in abdominal soft tissue surgery: technological overview and perspectives”, International Journal of Computer Assisted Radiology and Surgery, 2012,7(4).

[15] Wolfgang Koele, Heinz Stammberger, Andreas Lackner, Pia Reittner, “Image guided surgery of paranasal sinuses and anterior skull base - Five years experience with the InstaTrak®-System”, Rhinology, 2002 Mar;40(1):1-9.

[16] Christopher Nafis, Vern Jensen, Lee Beauregard, Peter Anderson, “Method for estimating dynamic EM tracking accuracy of Surgical Navigation tools”, Proc. of SPIE Medical Imaging: Visualization, Image-Guided Procedures and Modeling, San Diego, CA, vol. 6141, pp. 152–167, 2006.

[17] Julian Much, “Error Classification and Propagation for Electromagnetic Tracking”, Technische Universität M¨unchen Fakultät für Informatik.

[18] D. D. Frantz, A D Wiles, S E Leis, S R Kirsch, “Accuracy assessment protocols for electromagnetic tracking systems”, Physics In Medicine And Biology. 48 (2003) 2241–2251.

[19] Suzanne LaScalza, Jane Arico, Richard Hughesa, “Effect of metal and sampling rate on accuracy of Flock of Birds electromagnetic tracking system”, Journal of Biomechanics 36 (2003) 141–144.

[20] Tomasz Bien, Georg Rose, “Algorithm for calibration of the electromagnetic tracking system”, IEEE-EMBS International Conference on Biomedical and Health Informatics (BHI 2012).

[21] Aurora Accuracy Performance – Planar Field Generator. [Online]. S
Available: https://www.ndigital.com/medical/products/aurora [Accessed Apr. 10, 2019]

[22] F. Attivissimo, A. Di Nisio, A.M.L. Lanzolla, P. Larizza, S. Selicato, “Evaluation of noise performance of an electromagnetic image-guided surgery system,” in Proc. IEEE International Instrumentation and Measurement Technology Conference, pp. 6, May 14-17, 2018, Houston, USA.

[23] F. Attivissimo, A.M.L. Lanzolla, S. Carlone, P. Larizza, G. Brunetti, “TDM-FDM configuration of electromagnetic tracking system for image-guided surgery devices”, 2017 IEEE International Instrumentation and Measurement Technology Conference (I2MTC), Turin, 22-25 May 2017, pp 1-6.

[24] https://www.ndigital.com/medical/products/tools-and-sensors [Accessed Apr. 10, 2019]

[25] IEEE Standard for Safety Levels with Respect to Human Exposure to Electromagnetic Fields, 0-3 kHz, Std. C95.6-2002.

[26] IEEE Standard for Safety Levels with Respect to Human Exposure to Radio requency Electromagnetic Fields, 3 kHz to 300 GHz, Std. C95.1-2005, Revision of IEEE Std C95.1 -1991, 2006.

[27] F- Attivissimo, A. M. L. Lanzolla, S. Carlone, P. Larizza , G. Brunetti, “A novel electromagnetic tracking system for surgery navigation”, Computer Assisted Surgery, vol. 23, no.1, 2018. pp. 42-52.

[28] G. M. Nielson, H. Hagen, and H. Mu¨ller, Scientific Visualisation, IEEE, New York 1997.

[29] Amidror, Isaac. “Scattered data interpolation methods for electronic imaging systems: a survey.” J. of Electronic Imaging, vol. 11, no. 2, April 2002, pp. 157–176.